Microstructural Characteristics of Epitaxial $BaSrNb_{0.3}Ti_{0.7}O_3$ Film

Li'na CHENG and Xiuliang MA†

Shenyang National Laboratory for Materials Science, Institute of Metal Research, Chinese Academy of Sciences, Shenyang 110016, China

[Manuscript received April 29, 2007, in revised form June 6, 2007]

Microstructural characteristics in the $BaSrNb_{0.3}Ti_{0.7}O_3$ thin film, grown on $SrTiO_3$ substrate by computer-controlled laser molecular beam epitaxy, were characterized by means of transmission electron microscopy (TEM). It is found that the film is single-crystallized and epitaxially grown on the $SrTiO_3$ substrate forming a flat and distinct interface. Anti-phase domains were identified, and the crystallographic features of mismatch dislocations at the interface between film and substrate were clarified. The high conductivity of the present film was discussed from the viewpoint of Nb dopant and the nitrogen atmosphere.

KEY WORDS: $BaSrNb_{0.3}Ti_{0.7}O_3$ thin film; Epitaxial growth; Transmission electron microscopy

1. Introduction

The intense studies devoted to oxide thin films with the perovskite-based structure in recent years have been motivated by their widely potential application in memory devices, multilayer capacitors, electro-optic devices, and infrared detectors, and *etc*[1–6].

Owing to the large band gap and closed shell configuration, stoichiometric $BaTiO_3$ (BTO) is an insulator. However, both reduction ($BaTiO_{3-x}$) and impurity doping can induce the semiconducting behaviour. For instance, it has been found that a rich variety of physical properties such as good electrical and optical properties are produced by Nb doping in $BaTiO_3$[7]. When doped with Nb^{5+}, some free electrons are introduced into the film with Nb^{5+} substituted for Ti^{4+} and therefore the doped $BaTiO_3$ becomes an n-type semiconductor. The crystallographic and photoelectric properties of the doped BTO thin films have been studied by several groups[6–12]. It was found that the lattice parameters of $BaNb_xTi_{1-x}O_3$ increase linearly with increasing the content of Nb doping. The c/a ratio of $BaNb_xTi_{1-x}O_3$ tetragonal structure is less than that of stoichiometric BTO. In addition, the magnitude of electrical resistance of doped BTO thin film was reduced to 6.05×10^{-5} Ω·cm[11]. However, up to date, the microstructures of the doped BTO thin film grown in variant atmospheres have not yet extensively studied.

In the present study, we investigate the microstructure and defect configuration in the $BaSrNb_{0.3}Ti_{0.7}O_3$ film by various TEM (transmission electron microscopy) techniques, including conventional TEM and high-angle annular dark-field (HAADF) imaging.

2. Experimental

$BaSrNb_{0.3}Ti_{0.7}O_3$ thin films with the thickness of about 200 nm were deposited on $SrTiO_3$ (STO)(001) substrate by computer-controlled laser molecular beam epitaxy (LMBE). $BaSrNb_{0.3}Ti_{0.7}O_3$ target was used in the whole growing process under the nitrogen condition (P_{N_2}) of 10^{-1} Pa. During the growth of the film, a focused pulsed laser beam of two-dimensional scanning was impinged onto the two targets with a frequency of 2 Hz and an energy density of about 1 J/cm^2. The deposition rate was about 0.01 nm/pulse. Both cross sectional and plan view specimens for TEM observation were prepared by conventional process such as slicing, grinding and finally ion-milling. A JEOL 2010 high-resolution transmission electron microscope (HRTEM) with point resolution of 0.194 nm, working at 200 kV, was used to carry out contrast analysis and lattice imaging. A Tecnai G^2 F30 transmission electron microscope, equipped with HAADF detector, was used for Z-contrast imaging.

3. Results and Discussion

Figure 1(a) is a low magnification cross-section TEM image showing the morphology of the $BaSrNb_{0.3}Ti_{0.7}O_3$ film grown on $SrTiO_3$ substrate. It can be clearly seen that the interface is sharp and flat. The thickness of the film is about 200 nm. Columnar bands with dark contrast can be found in the film. These columnar structures originate from the interface between the film and substrate and extend to the surface of $BaSrNb_{0.3}Ti_{0.7}O_3$ film along the direction perpendicular to the interface. Figure 1(b) is a selected area electron diffraction (SAED) pattern corresponding to Fig.1(a). Such a diffraction pattern taken at the interface between the $BaSrNb_{0.3}Ti_{0.7}O_3$ film and STO substrate is a superposition of two sub-patterns, which comes from both $BaSrNb_{0.3}Ti_{0.7}O_3$ film and STO substrate. No extra spots can be identified from the pattern, indicating that no secondary phase in the film. According to the diffraction pattern, the $BaSrNb_{0.3}Ti_{0.7}O_3$ film and STO substrate have parallel orientation relationship, such as $[100]_{\rm film}//[100]_{\rm STO}$, $[010]_{\rm film}//[010]_{\rm STO}$. The splitting of diffraction spots particularly high-index spots, as seen in Fig.1(c), indicates the difference of lattice parameters between film and substrate. It is found that the lattice parameters of $BaSrNb_{0.3}Ti_{0.7}O_3$ film are larger than those of STO substrate.

Figure 2(a) is an HRTEM image showing the interface characteristics between the $BaSrNb_{0.3}Ti_{0.7}O_3$ film and STO substrate, which was imaged along the [100] direction of STO substrate. The interface is

† Prof., Ph.D., to whom correspondence should be addressed, E-mail: xlma@imr.ac.cn.

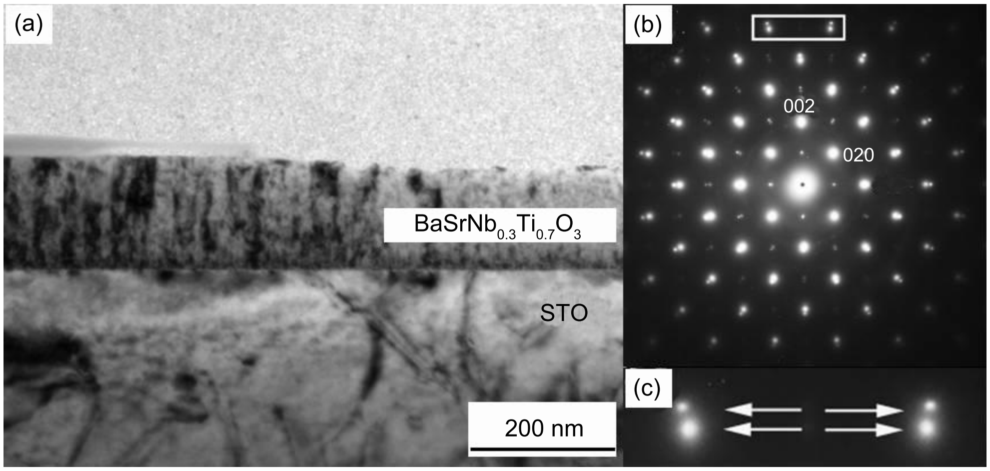

Fig.1 (a) Low magnification bright-field TEM image of $BaSrNb_{0.3}Ti_{0.7}O_3$ film grown on STO substrate, (b) the corresponding selected area electron diffraction pattern of the cross-section specimen with incident electron beam parallel to the [100] direction of STO substrate, (c) the enlargement of the rectangle in (b) showing the splitting of diffraction spots marked with arrows

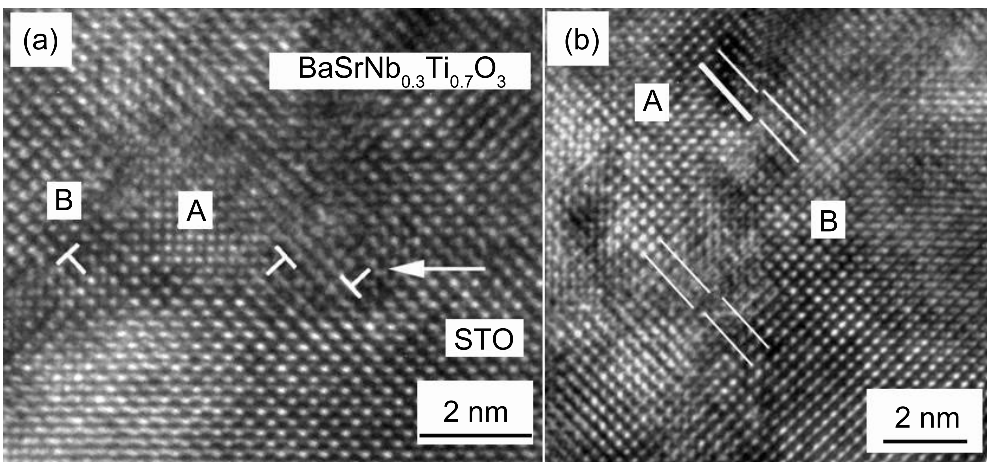

Fig.2 (a) HRTEM micrograph of the interface between the $BaSrNb_{0.3}Ti_{0.7}O_3$ film and STO substrate along the [100] direction of STO substrate, (b) HRTEM image with the $BaSrNb_{0.3}Ti_{0.7}O_3$ film showing the anti-phase domains

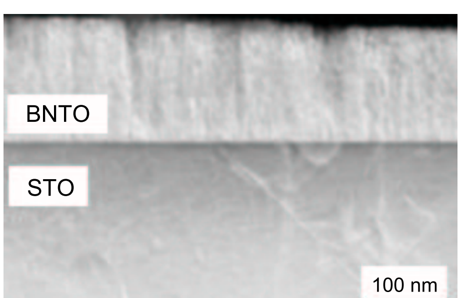

Fig.3 Low magnification HAADF image of the $BaSrNb_{0.3}Ti_{0.7}O_3$ film grown on STO substrate

indicated with an arrow. Neither elemental diffusion nor chemical reaction along the interface can be found. It is noted that misfit dislocations are observed along the interface, as marked in this image. Anti-phase domains marked with A and B in this image are found in the area near the interface. Figure 2(b) is an HRTEM image which was obtained within the $BaSrNb_{0.3}Ti_{0.7}O_3$ film. The anti-phase characteristics are marked with short bars in the domains labeled with A and B. Such domain structures are believed to correspond to the dark bands in Fig.1(a).

HAADF mode in a transmission electron microscope provides incoherent images, which uses high angle scattering and leads to strong atomic numbers (Z) associated contrast. The intensity of atom columns directly relates to the chemical composition. Figure 3 shows a low magnification cross section HAADF image of $BaSrNb_{0.3}Ti_{0.7}O_3$ film, in which the interface is evident. The film shows nearly homogeneous composition distribution though some areas reveal a little bit darker contrast in this image, which may result from the different thickness, as evidenced by the broken edges of the surface.

Besides the above features within the film, the lattice misfit relaxation mechanisms in heteroepitaxial growth structures are another important issue due to the potential influence of residual strains on the electrical and other physical properties. Figure 4(a) is a low magnification HRTEM image of the interface between the $BaSrNb_{0.3}Ti_{0.7}O_3$ film and STO substrate

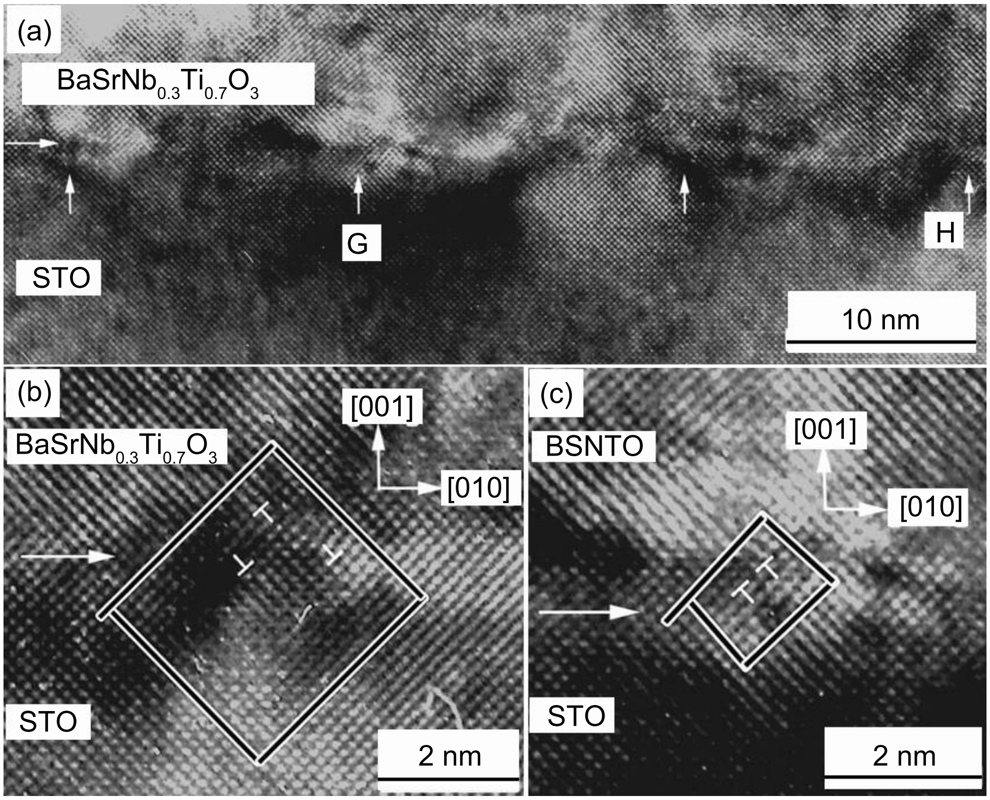

Fig.4 (a) Low magnification high-resolution image of the interface showing an approximately periodic array of mismatch dislocations, (b) an enlargement of the area signed with H in (a) showing the dislocation on the interface, (c) an enlargement of the area signed with G in (a) revealing a case of dislocation decomposition at the interface

taken along the [100] direction of STO substrate. It can be seen that an array of dislocations is nearly periodically distributed along the interface. Such misfit dislocations are denoted by upward arrows. The average spacing between two adjacent dislocations is about 16 nm. In order to get more information about the dislocation character, a mismatch dislocation denoted with H in Fig.4(a) is enlarged as seen in Fig.4(b), where the Burgers-circuit surrounding this dislocation core is drawn. There are three partial dislocations in this circuit. Two of them show opposite signs and counteract each other. The Burgers vector $\boldsymbol{b}$ is finally determined as $\boldsymbol{a}/2[0\bar{1}\bar{1}]$. Since the vector is not a lattice translation vector and no other related defects are found in the nearly area, the measured value must be the projected component of a perfect dislocation. He *et al.*[13] studied the misfit dislocations in $La_{0.7}Ca_{0.3}MnO_3$ thin films grown on $SrTiO_3$ by PLD (pulsed laser deposition). They found that a misfit dislocation with a projected Burgers vector $\boldsymbol{a}/2[1\bar{1}0]$ is the projected component of the perfect dislocation with the Burgers vector of $\boldsymbol{a}[010]$. In our case, we think that the partial dislocation should also be a projected component of a perfect dislocation with Burgers vector of either $\boldsymbol{a}[010]$ or $\boldsymbol{a}[001]$. Such dislocation configuration appears frequently along the interface. Detailed investigation is underway. Figure 4(c) is an enlarged image of the area marked with G in Fig.4(a), revealing another case of dislocations distribution. In this case, the dislocation is a perfect one and the closure failure leads to the Burgers vector $\boldsymbol{b}$ of $\boldsymbol{a}[011]$. It is worthy noting that the dislocation is further dissociated into two identical partials, which is similar to the results obtained in Nb-doped $SrTiO_3$ grown on $SrTiO_3$ by L-MBE (laser beam epitaxy deposition) technique[14]. The lattice mismatch (f) between the film and the substrate can be calculated based on the split of diffraction spots in the electron diffraction patterns. Accordingly, the separation of mismatch dislocations can be estimated to be 22 nm, based on the equation of $S=b/f$. Experimentally, the spacing of mismatch dislocations as seen in Fig.4(a) is less than that of calculation, which indicates that the misfit strain in the thin film system is not fully relaxed by the formation of misfit dislocations. Other relaxation mechanisms may also contribute to the relaxation process.

From plan view observation, we can get more useful information on microstructure of this film. Figure 5 is a low-magnification plan-view image showing the distribution of the anti-phase domain boundaries in the film. It can be observed that high density of anti-phase domains exist in the film. The domain boundaries reveal a wave-like pattern. The formation of anti-phase domains may also make contribution to the misfit strain relaxation in this heteroepitaxial system.

The film of $BaSrNb_{0.3}Ti_{0.7}O_3$ in the present study was grown under the condition of 10^{-1} Pa P_{N_2} and displays higher conductivity comparing with the film grown under the condition of 6.0×10^{-1} Pa P_{O_2}. Although Nb atoms are easy to be oxidized to become the stable phase Nb_2O_5, the probability of this oxidation reaction is less under low oxygen pressure[12].

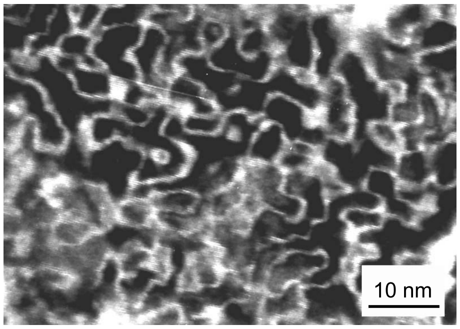

Fig.5 Low-magnification plan-view image showing the distribution of the antiphase domain boundaries in the film

Certainly, there is little probability to form Nb_2O_5 in our sample prepared without O_2 supply, which is also verified by the EDP (electron diffraction pattern). Hence, Nb doping is a noteworthy factor that is beneficial to increasing the electrical conductivity of the film in this study. More free electrons will be imported when Nb^{5+} ions substitute Ti^{4+} ions more efficaciously. In addition, the whole deposition process is carried out under the condition of reducing atmosphere of N_2. According to defect chemistry theory, the presence of nitrogen causes the increase of charge carrier. Besides, almost none of threading dislocations is observed in the $BaSrNb_{0.3}Ti_{0.7}O_3$ film. It is known that presence of threading dislocations usually cumbers the transport of charge carrier and leads to the decrease of electron mobility. So from the microstructure point of view, the low density of threading dislocations is likely to be an important reason that makes the $BaSrNb_{0.3}Ti_{0.7}O_3$ film highly conductive.

4. Conclusion

Microstructural characteristics of highly conductive $BaSrNb_{0.3}Ti_{0.7}O_3$ film have been characterized by transmission electron microscopy. Anti-phase domain boundaries are found in the film with high density. An array of misfit dislocations with different configurations is observed nearly periodically distributing along the interface between the film and substrate. Together with Nb dopant and the nitrogen atmosphere, it is proposed that the low density of threading dislocations contributes to high conductivity of the $BaSrNb_{0.3}Ti_{0.7}O_3$ film.

Acknowledgements

We thank Professor H.B.Lu, Institute of Physics, Chinese Academy of Sciences, China for help with the thin film preparation. This work was supported by the National Natural Science Foundation of China under Grant No. 50325101 and the Special Funds for the Major State Basic Research Projects of China (Grant No. 2002CB613503).

REFERENCES

[1] J.G.Bednorz and K.A.Muller: *Z. Phys. B,* 1986, **64,** 198.
[2] C.W.Chu, H.P.Hor, R.L.Meng, L.Gao and Z.J.Huang: *Science,* 1987, **235,** 567.
[3] M.Sayer and K.Screenivas: *Science,* 1990, **247,** 1056.
[4] R.E.Cohen: *Nature,* 1992, **358,** 136.
[5] R.Von Helmolt, J.Wecker, B.Holzapfel, L.Schults and K.Samwer: *Phys. Rev. Lett.,* 1993, **71,** 2331.
[6] H.Z.Guo, L.F.Liu, H.B.Lu, Y.Y.Fei, W.F.Xiang, Y.L.Zhou and Z.H.Chen: *Chin. Phys. Lett.,* 2004, **21,** 396.
[7] L.T.Hudson, R.L.Kurtz, S.W.Robey, D.Temple and R.L.Stockbauer: *Phys. Rev. B,* 1993, **47,** 1174.
[8] D.Nagano, H.Funakubo, K.Shinozaki and N.Mizutani: *Appl. Phys. Lett.,* 1998, **72,** 2017.
[9] M.T.Buscaglia, V.Buscaglia, M.Viviani, P.Nanni and M.Hanuskova: *J. Eur. Ceram. Soc.,* 2000, **20,** 1997.
[10] Y.Kim, C.H.Chen, A.Saiki, N.Wakiya, K.Shinozaki and N.Mizutani: *J. Phys. D Appl. Phys.,* 2002, **35,** 1499.
[11] L.Yan, H.B.Lu, Z.H.Chen, S.Y.Dai, Y.L.Zhou and G.Z.Yang: *J. Cryst. Growth,* 2002, **244,** 225.
[12] T.Tomio, H.Miki, H.Tabata, T.Kawai and S.Kawai: *J. Appl. Phys.,* 1994, **76,** 5886.
[13] J.Q.He, C.L.Jia, J.Schubert and R.H.Wang: *J. Cryst. Growth,* 2004, **265,** 241.
[14] Y.L.Zhu, X.L.Ma, D.X.Li, H.B.Lu, Z.H.Cheng and G.Z.Yang: *Acta Mater.,* 2005, **53,** 1277.